HiSST: 2nd International Conference on
High-Speed Vehicle Science & Technology

11–15 September 2022, Bruges, Belgium

Multi-Functional Multi-Lobe Optimization of Cryogenic Fuel Tank Structures for Hypersonic Vehicles

Miguel Rodriguez-Segade [1], Johan Steelant[2], Santiago Hernandez[3] and Jacobo Diaz[4]

Keywords: *hypersonic, structures, cryogenic tanks*

1. Introduction

Slender hypersonic craft have potential applications ranging from point-to-point transportation to low-cost reusable access to space. For civil transportation, they are considered as the future technology for high-speed commercial travel to any location of the planet in less than four hours. The successful design of a cruising hypersonic aircraft will depend on a detailed balance between structural design, aerodynamics, and propulsion.

Two major challenges when designing hypersonic vehicle within the air atmosphere are the thermal management and structural capacity. Regarding thermal management, the aeroshell geometry determines the heat fluxes. In contrast to hypersonic blunt-body capsules, cruise vehicles require a higher L/D ratio, hence exhibiting a more slender shape. As a result, heat is dissipated through near-wall phenomena along the wetted surface instead of strong bow shocks that would mainly heat the stagnation area. For this reason, there is significantly more surface area that needs to be handled by the thermal protection system. Beyond that, a sound structural design requires subsystems to be tightly integrated within the airframe. Specifically, the fuel tanks must be accommodated to the external aerodynamic surfaces and internal propulsive flowpaths, seeking an efficient compromise between internal volume and structural weight. This multi-functionality can be achieved using the multi-lobe concept, which is a promising solution for novel vehicle architectures [1].

In Europe, several projects were involved in the design of a hypersonic cruise vehicle. The LAPCAT MR2.4 vehicle [2] consists of a waverider lifting-body with an integrated dorsal-mounted propulsion system. To be efficient during hypersonic cruise, the vehicle has leading edges with small radius to ensure good aerodynamic efficiency (L/D). Fig. 1 shows the external skin of the aircraft, which can be divided into a center fuselage section that contains the propulsive flowpath, and the delta wings.

Based on the design of the LAPCAT MR2.4 vehicle, the STRATOFLY MR3 was developed a few years later. Fig.2b shows a comparison between the tank arrangements of the two vehicles. The STRATOFLY MR3 contains gaps between some of the lobes to allow sufficient space for the landing gears and cabin entrances. This solution was found to have flaws [3] and thus heavier than the one used for the LAPCAT MR2.4 [4]. Therefore, an optimum continuous set of lobes from the tip to the end of the wing is sought in this research, following the idea proposed during the LAPCAT project (Fig. 2a).

Although previous studies have shown promising results for this concept [5], a detailed study is needed to analyze the benefits of the different multi-lobe configurations. In this sense, this research proposes an optimization study to obtain the best multi-lobe configuration as an integral solution for a hypersonic vehicle.

2. Hydrogen tanks for hypersonic vehicles

The overall objective of a hypersonic vehicle tank design is to have a safe, lightweight, thermally efficient storage system. Hydrogen can be stored as a compressed gas (CGH2) or as a liquid (LH2). CGH2

[1] *University of A Coruna, Structural Mechanics Group, miguel.alonso1@udc.es*
[2] *ESTEC-ESA, Flight Vehicle and Aerothermodynamics Engineering Section*
[3] *University of A Coruna, Structural Mechanics Group*
[4] *University of A Coruna, Structural Mechanics Group*

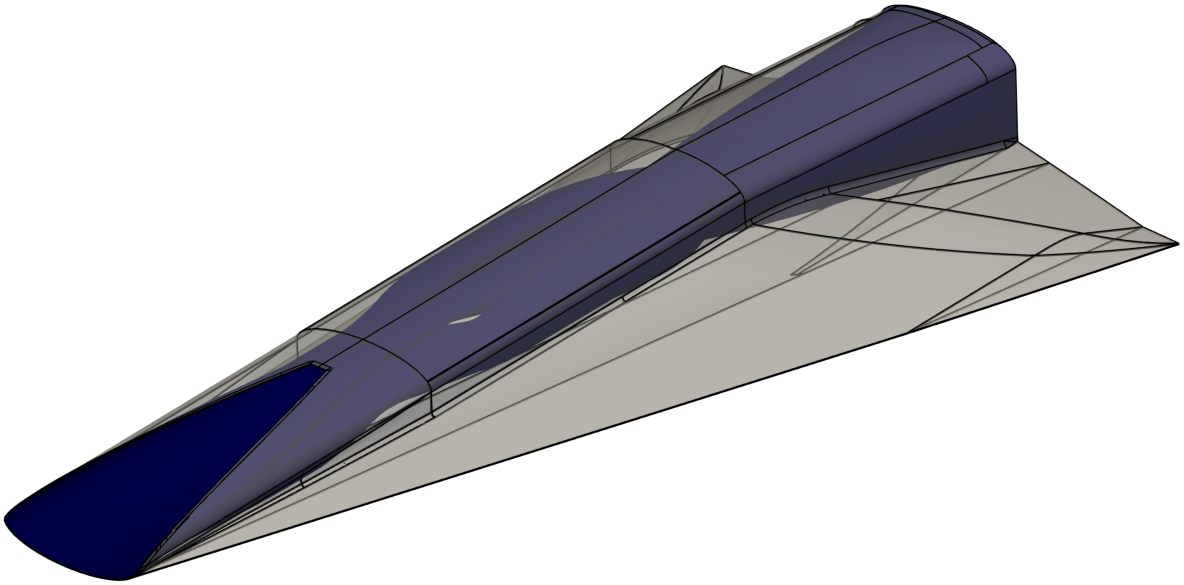

Fig 1. LAPCAT main external aerodynamic surfaces and internal flowpath highlighted in blue

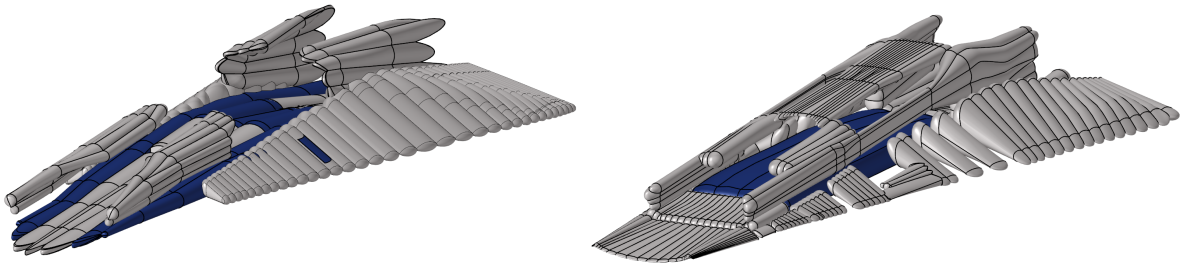

(a) LAPCAT multi-lobe arrangement **(b)** STRATOFLY multi-lobe arrangment

Fig 2. Differences between the LAPCAT and STRATOFLY internal configurations

needs to be highly compressed to store the highest amount of energy in a given volume. Although CGH2 tanks are currently under development by other engineering disciplines, such as the automotive field [6], these concepts are not applicable to an aircraft. The need of larger tanks to accommodate the required on-board fuel would imply a heavier design able to meet the strength requirements. As an alternative, the temperature of the hydrogen can be reduced until reaching the liquid state, which requires smaller and lighter tanks due to the significantly lower pressures to accommodate the required fuel mass.

One of the predominant technological barriers when designing liquid hydrogen powered aircraft is storing enough hydrogen mass onboard to achieve a sufficient range for the mission. Although it possesses higher specific energy (energy per unit mass) than other jet fuels, cryogenic hydrogen has significantly less energy density (energy per unit volume), which implies lightweight but large volumes to be integrated within the airframe.

Regarding the material selection, fiber reinforced composites are not considered a option due to the permeability of the resins. When this material is subjected to high strains resulting from mechanical and thermal loads, it is no longer capable of holding the hydrogen without significant losses. In addition, the thermal cycling associated with repeated filling and draining may cause material fatigue damage in the form of matrix microcracking, which may result in further leakage [7]. For these reason a linerless tank of a dense metallic material was opted in this study as first choice and to work out a methodology to minimize cost, weight, and compatibility issues.

Large lightweight tanks would collapse due to the compressive forces caused by their own weight, unless there is an internal pressure that can induce tensile forces to counteract this effect, preventing buckling. For this reason, LH2 tanks with large size and relatively small thickness need an internal pressure to be stable. This is the case in a study conducted by Steelant et al. [8], an internal overpressure of 0.5 bar was used for the LAPCAT MR2 cryogenic tanks. This value will be used in the tank analysis herein.

3. Two-lobe tank configuration

As an illustrative example, the behaviour of a two bubble tank with a web subject to internal pressure forces is analyzed. The finite element model exclusively comprises quadrilateral elements without transverse shear deformations (Classical Plate Theory) [9]. The material is Aluminium 2187 with a T87 temper, which is considered to be one of the best materials for fabrication of manned spacecraft tankage [10]. The model consists of two consecutive lobes with identical radii (r) with an overlap defined by the intersection of angles ϕ and θ. At the intersection of the two lobes, vertical webs are disposed to transfer the circumferential hoop stresses from top to bottom. The connection between the skins and the web is usually referred to as a Y-junction due to its shape. Apart from being structurally efficient, this strategy has the additional benefit of reducing dynamic loads caused by the internal sloshing [11].

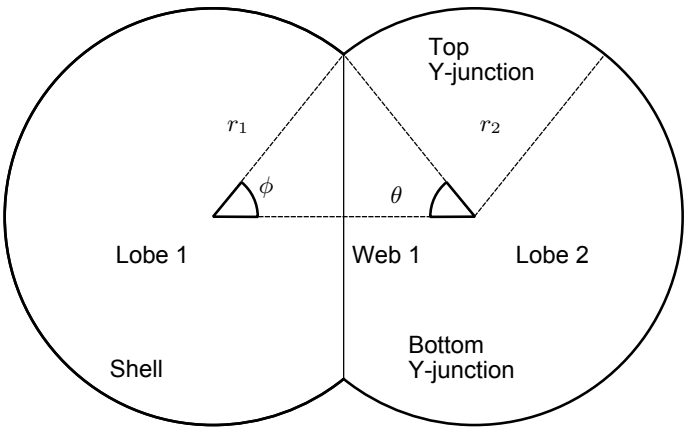

Fig 3. Parameters in two lobe definition

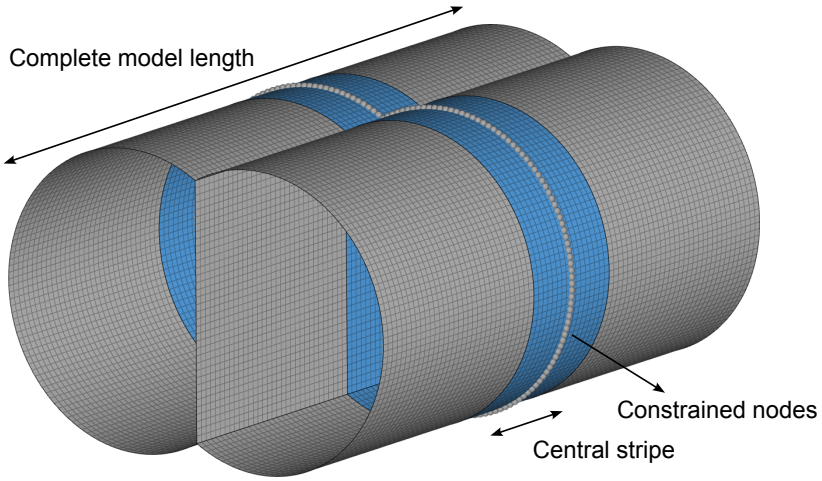

Fig 4. Model used to analyze the two lobe configuration, with the central stripe shown in blue

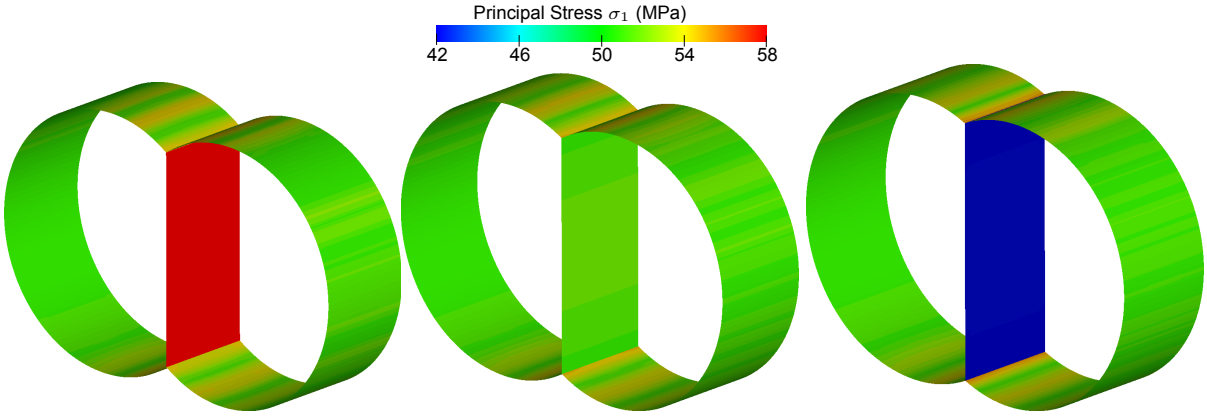

(a) $\phi = 55$ **(b)** $\phi = 60$ **(c)** $\phi = 65$

Fig 5. Different stress distribution for different angles $\phi = \phi_1 = \theta_1$

The model shown in Fig.4 is used to analyze the structural behaviour of the tank. The pressure applied has a value of 50 kPa, the length is 4 m and it was meshed using 0.05 m sized quadrilateral elements. The web and the shell have equal thicknesses of 1 mm. Results are only discussed in a 1 m wide stripe at the center of the model as shown in the Figure. The purpose is to capture the general behaviour of the tank and to avoid local effects at the border. The longitudinal and tangential displacements are constrained in the highlighted nodes. In this manner, the tank is able to freely deform without incurring in a stiffness matrix singularity.

Fig. 5 shows different stress distributions for different angles. As can be seen, the lower stress values are obtained with an angle of $\phi = 60°$; this is because the vertical components of the hoop stresses of the lobes balance out with the web tensile stress as shown in the free body diagram presented in Fig. 6, which depicts the membrane forces at the Y-junction. For two lobes of equal radii, the vertical equlibrium equation can be written as:

$$2N_\theta \cos\phi = N_w \tag{1}$$

Therefore, at the Y-junction, for $\phi = 60$, the web an the lobes should have exactly the same membrane axial stresses, but bending stresses propagate throughout the lobe. For this reason, instead of defining a single thickness for the entire tank, several patches need to be set for a more appropriate subdivision.

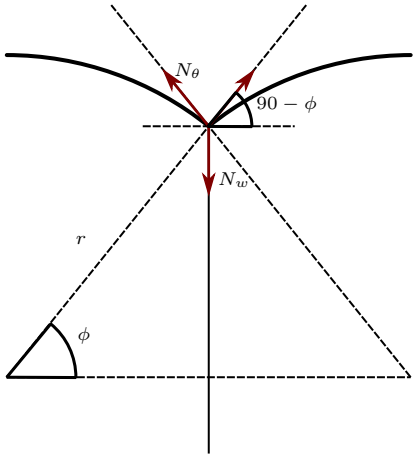

Fig 6. Force equilibrium at the Y-junction

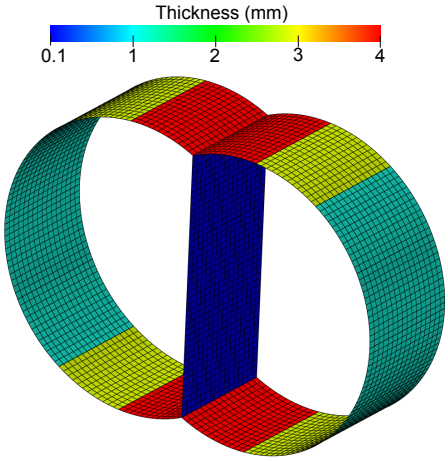

Fig 7. Preliminary optimization for a two lobe, $\phi = 60$ configuration with 8 thicknesses per lobe

Consequently, the thickness can be better adjusted resulting in a lighter design. By performing an optimization to minimize the weight in the $\phi = 60$ configuration, an improved thickness distribution is obtained, as shown in Fig. 7. If the number of thicknesses is increased we can reduce the weight even further. Going from 8 thicknesses per lobe to 32, the mass is reduced from 21.092 kg to 20.516 kg. But this approach will increase the complexity of the design, being necessary to choose a compromise solution between complexity and weight.

4. Parametric model

To assess the benefits and drawbacks of the different tank geometries, a parametric model able to obtain the mechanical behaviour of any arbitrary configuration is needed. To make this model robust, we chose a set of parameters that avoid impossible configurations. Furthermore, continuous variables are preferred, so that a gradient based optimization algorithm could be applied afterwards.

4.1. Definition of geometrical parameters

As mentioned previously, the main benefit of the multi-lobe configuration is to be able to adapt to any external geometry, e.g. a hypersonic wedge wing or a rounded waverider fuselage body. This is referred to in the literature as a conformal tank. To obtain a general approach, the top and bottom boundaries are considered as straight lines. Therefore in case of a curved boundary, the path will be approximated to a polygonal line.

The paremetrization approach is outlined in Fig. 8. Initially, the radius of each lobe was considered as a parameter, because the angles ϕ_i and θ_i, as well as the center of each lobe, could be obtained geometrically by imposing tangency at the top and bottom lines. However, this approach led to impossible, non-overlapping, strictly tangent or coincident configurations. In order to avoid all of these pitfalls, the problem was formulated from a different perspective. By fixing the initial and final lobes to be tangent to the top, bottom and corresponding side boundaries, the subsequent circles were defined by a parameter pr_i. This parameter represents the overlap between the current lobe and the previous one, lying between lb_i and rb_i, which act as margins to avoid coincident and tangent lobes. The overlap value pr_i is expressed as a percentage of its domain, because the interval $[lb_i, rb_i]$ depends on the previous values of pr_i, and can not be known *a priori*.

An important caveat is not knowing how many lobes a given configuration will produce. To address this, a sufficiently large number of pr_i parameters is provided, and the circles are created sequentially until there is no more space left. In this sense, we could provide as parameters n values of pr_i but only a fraction $m < n$ of circles will be included in the design.

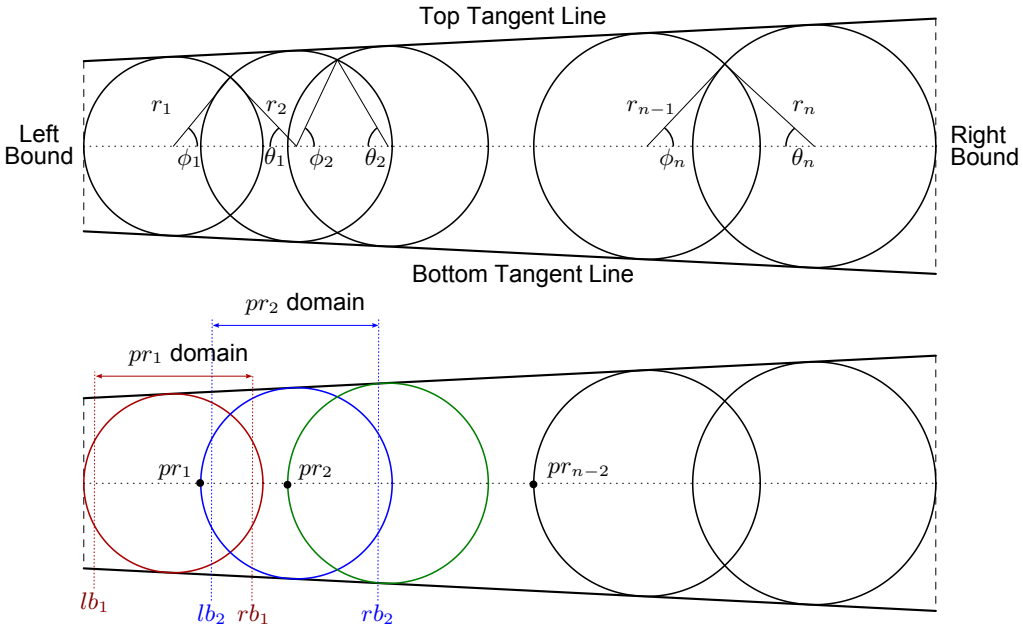

Fig 8. Different sets of parameters used to the define the multi-lobe configuration

The pr_i parameters define three lines tangent to each circle, as shown in Fig. 9. From these lines, the geometrical values r_i, ϕ_i, θ_i, and the center c_i, of each circle can be calculated. If the two oblique lines are symmetric with respect to the x-axis and defined through the equations $y_1 = ax + b$ and $y_2 = -ax - b$, and the vertical line is defined through the equation $x = d$, then:

$$c_i = \frac{d\sqrt{a^2+1} - b}{a + \sqrt{a^2+1}} \qquad r_i = \frac{da + b}{a + \sqrt{a^2+1}} \tag{2}$$

and the intersection angles can be obtained applying the cosine law in the triangle formed by the two radii and the distance between the centers $\Delta c = c_{i+1} - c_i$:

$$\cos\phi_i = \frac{\Delta c^2 + r_i^2 - r_{i+1}^2}{2\Delta c r_i} \qquad \cos\theta_i = \frac{\Delta c^2 + r_{i+1}^2 - r_i^2}{2\Delta c r_{i+1}} \tag{3}$$

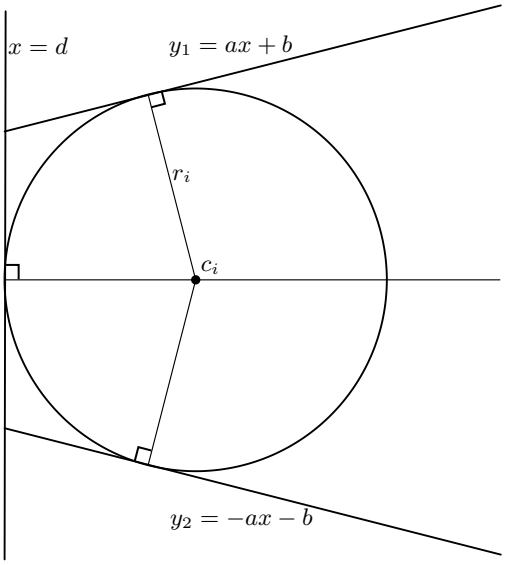

Fig 9. Circle tangent to 3 lines

4.2. Finite element model

Once the geometry is completely defined, a meshing strategy has to be employed. To do so, each lobe and web is subdivided in the required number of arches and extruded through the length of the tank. The resulting surfaces are meshed through a transfinite mapping algorithm [12] obtaining a compatible and high quality mesh. To generate the model in a systematic fashion a reliable numbering system has to be put into place. Fig. 10 shows the patches and numbering system of a four lobe design, with four patches on the boundary cylinders, two in the intermediate ones, and three on each web.

The boundary conditions are imposed on the center section of each lobe in the same manner as previously explained in Fig. 4. Regarding the loads, the internal pressure and the external aerodynamic forces produced by the high-speed velocity regime are imposed. Fig. 11 shows a side view of the wing of the LAPCAT vehicle. The slender shape produces oblique shock waves at the bottom of the vehicle, and a Prandtl-Meyer expansion fan at the convex corner of the top surface. The bottom shock increases the aerodynamic pressure, which can be obtained using local Rankine-Hogoniot shock wave equations.

5. Optimization strategy

The optimization problem is formulated to solve the question of what is the optimal multi-lobe configuration that provides the maximum internal volume while maintaining structural strength and stability. Although a conformal tank solution would have the maximum fuel capacity, it is not the most structurally efficient. For that reason, a trade-off between weight and volumetric efficiency must be sought.

To define design variables that control the number and shape of lobes, as well as the thicknesses of the skin and webs. Hereby we denote M as the mass of the tank, *Vv* the void volume or volume without fuel, as shown in Fig. 12, σ_j^{Von} the Von Mises stress and λ_1 the first buckling eigenvalue. The vector of design variables is composed by the overlap between the bubbles, **p**, as defined in Fig. 8; and the thicknesses, **t**.

The problem is challenging for the following reasons:

- The number of lobes is a discrete variable, so no continuous optimization technique can be directly applied
- There are a lot of impossible configurations that could make the optimization algorithm unstable

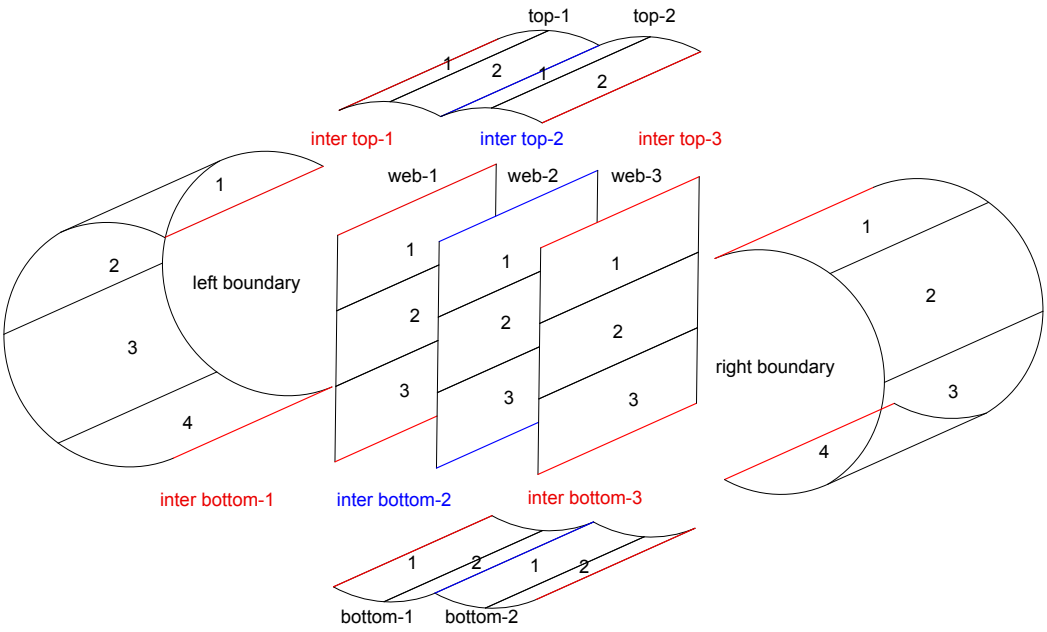

Fig 10. Tank module numbering system

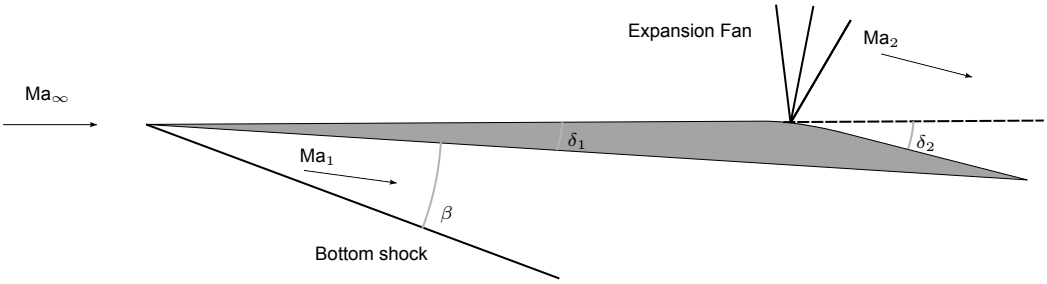

Fig 11. Hypersonic wing loads

- The number of design variables is not constant, this is because, if the number of lobes increases, the number of design thicknesses also increases Furthermore, the size of the Jacobian would not be constant through the optimization process.

The first two issues can be solved by using the parametric model defined in the previous section, as it converts the discrete variables in a series of continuous variables that cannot produce problematic designs. The final concern is addressed by dividing the optimization problem in two levels, one level with as much design variables as possible lobes, and the other one with the required number of thicknesses for the proposed configuration. The complete approach can be divided into two main steps, denoted as global and local search, which are explained in detail in the following sections.

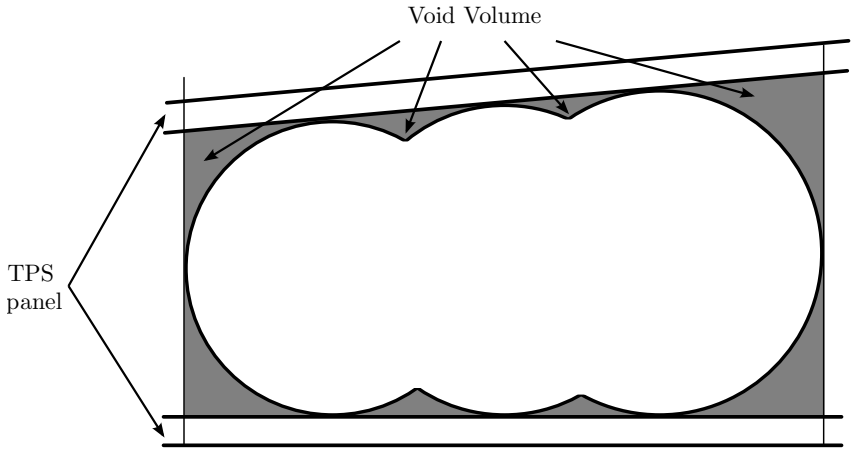

Fig 12. Void volume

5.1. Global search

An additional difficulty encountered during the development of the methodology lies in the fact that the optimization problem has many local minima, and the behaviour changes drastically when additional lobes are incorporated or removed from the design. For this reason any local search algorithm will only find optimum solutions near the initial design, and will not explore configurations with different number of lobes. To overcome this obstacle, a derivative-free algorithm was chosen that sufficiently samples the design space to explore all possible solutions.

The parametric model was incorporated into an optimization problem organized in two optimization levels: the outer level corresponds to the genetic algorithm, which is in charge of proposing a new population based on the overlap between lobes. Then, at the inner level, the parametric model is built according to the characteristics of each individual in the population. Each model is optimized using a gradient-based algorithm, considering as design variables the thicknesses of the shell elements. As a result, a pair of values - volume capacity vs. weight - is obtained for each individual, which are ranked by the genetic algorithm. Then, a new population is proposed and the process is repeated. When the maximum number of evaluations is reached, the process is terminated, and the non-dominated designs are selected and passed as inputs to the next step.

5.2. Local search

For each non-dominated design of the previous step, a final local optimization is performed in a single level. In this step the mass and the void volume are weighted into a single objective function. A gradient-based algorithm is employed, where the side constraints of the thicknesses are tightened, so that the number of lobes does not vary. For the algorithm to be efficient, all gradients must be provided to the optimizer [13]. The four required derivatives are calculated as follows: (1) the derivatives of the mass with respect to the thickness $\frac{\partial M}{\partial \mathbf{t}}$ are obtained by the structural sensitivity analysis, (2) the derivatives of the void volume with respect to the overlap parameters $\frac{\partial V_V}{\partial \mathbf{p}}$ are obtained by algorithmic differentiation [14], since the void volume is calculated using standard `python` functions, (3) the derivatives of the

void volume respect to the thicknesses $\frac{\partial \mathit{Vv}}{\partial \mathbf{t}}$ are assumed to be 0, and (4) the derivatives of the mass respect to the overlap parameters $\frac{\partial M}{\partial \mathbf{p}}$ are obtained with the following relation, as the design variables are independent among them:

$$M = L \sum \mathit{Pe}_i t_i \implies \frac{\partial M}{\partial \mathbf{p}} = L \sum \frac{\partial \mathit{Pe}_i t_i}{\partial \mathbf{p}} = L \sum \frac{\partial \mathit{Pe}_i}{\partial \mathbf{p}} t_i \tag{4}$$

being Pe_i the perimeter of each patch along the cross-section. The derivatives of the perimeter with respect to the overlap parameters $\frac{\partial \mathit{Pe}_i}{\partial \mathbf{p}}$ are also obtained via algorithmic differentiation. The optimization problem can be formulated as follows:

$$\begin{aligned}
&\min \ \alpha \frac{M^q}{M_0^q} + (1-\alpha)\frac{\mathit{Vv}^q}{\mathit{Vv}_0^q} && \text{(5a)}\\
&\text{s. t.} \qquad M^q < M_0^q && \text{(5b)}\\
&\qquad\quad \mathit{Vv}^q < \mathit{Vv}_0^q && \text{(5c)}\\
&\qquad\quad \sigma_j < \sigma_{\text{max}} && \text{(5d)}\\
& && \text{(5e)}
\end{aligned}$$

where α represent the weighting parameter to perform the multi-objective optimization. The value of this parameter can be approximated as the horizontal or vertical distance to the normalized utopia point. In this manner, the previously obtained design is improved and some designs can even match. Once the process is completed, the final Pareto front is obtained. The flowchart of the two steps are depicted in Fig. 13. The methodology was implemented using a variety of software tools and libraries. The process is summarized in Fig. 14.

6. Results

In this study we optimized the tank configuration inside the section of a wedge defined by the lines indicated in Fig.9 with equations: $y_1 = 0.05x + 1.0$ and $y_2 = -0.05x - 1.0$ from $x = 0$ to a width of 10 m. This implies a total clearance between 2 m (left bound) and 3 m (right bound). Each model generated was automatically meshed with an element size of 0.05 and subdivided with eight patches on the boundary lobes, four on the intermediate ones, and three on the webs. In the longitudinal direction, the model is partitioned in five modules, but only the results of the central one are discussed. The aerodynamic loads correspond to a cruise condition at an altitude of $35\,000$ m, $\mathit{Ma} = 8$, and $0°$ angle of attack. The material is Aluminum 2219-T87 with a Young modulus of 85 GPa, yield stress of 476 MPa, poisson ratio of 0.33, and density of $2840\,\text{kg}/\text{m}^3$.

The initial design of the optimization corresponds to equal overlap parameters of 0.1 and thicknesses of 1 mm. The global search approach was limited to 2500 model evaluations. All the mass and void volume values are shown in Fig.15. It is clear from the results that the values are organized in clusters corresponding to the number of lobes, albeit there are some outliers that correspond to very poor designs.

Extracting the list of non-dominated designs, we obtain five configurations that are used as starting points for the last step. As can be seen in Fig.16, the three designs of nine lobes coalesce to a single optimum design, and the five and six lobes solutions are slightly improved.

The number of lobes, M^*, and Vv^* are summarized in Table 1. In addition, the lobe, thickness, and stress distribution are presented in Figs. 17, 18, and 19, respectively.

Analyzing each optimum design, it is observed that the most volumetrically efficient are those with more lobes, but they correspond to the heaviest designs. In contrast, the lightest designs are the ones with less lobes. The mass varies 5.0% across the Pareto front, and the available volume to almost 120%. Calculating the ratio of mass to void volume, the most efficient design is among the cluster of the heavier

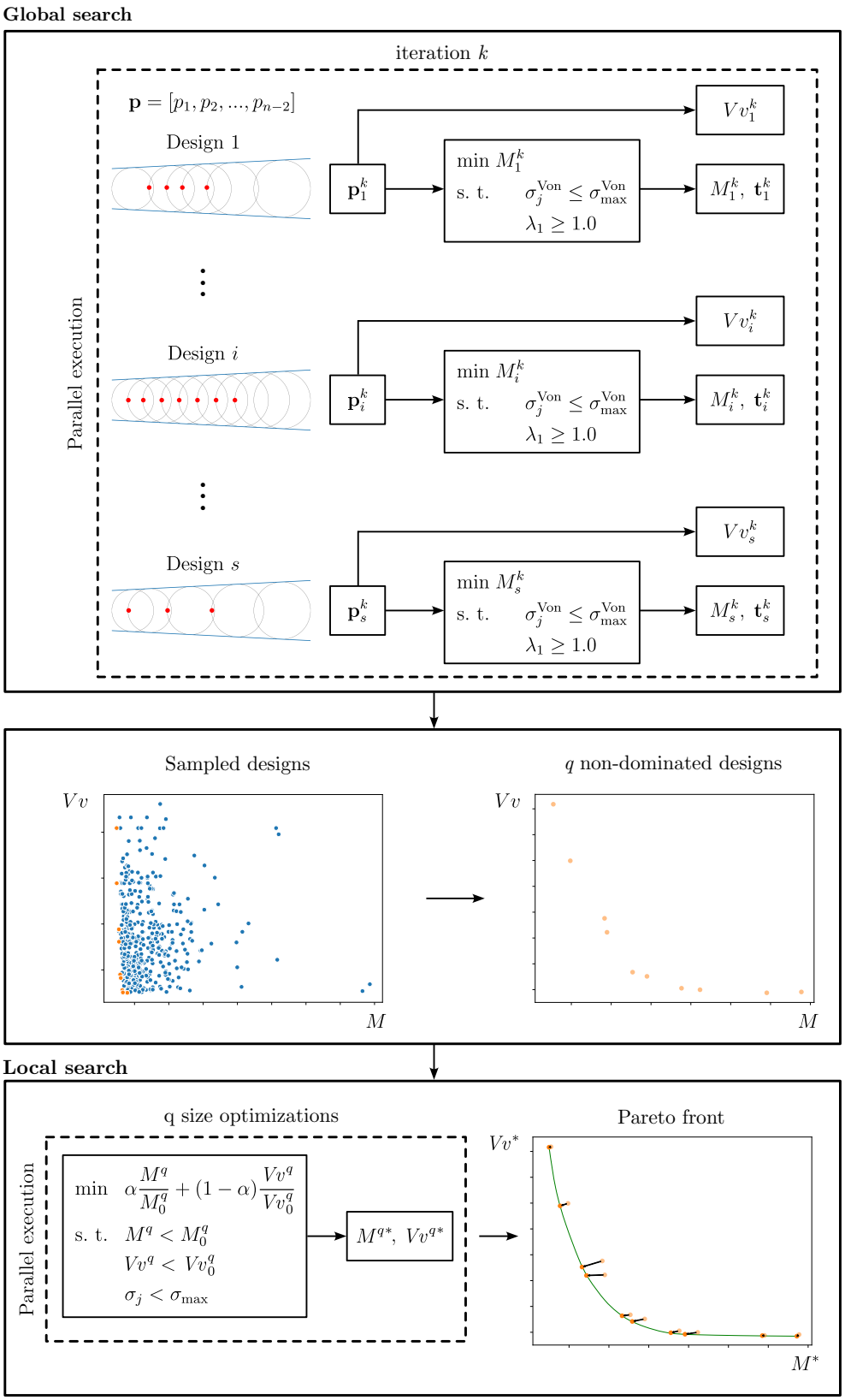

Fig 13. Flowchart of the optimization process

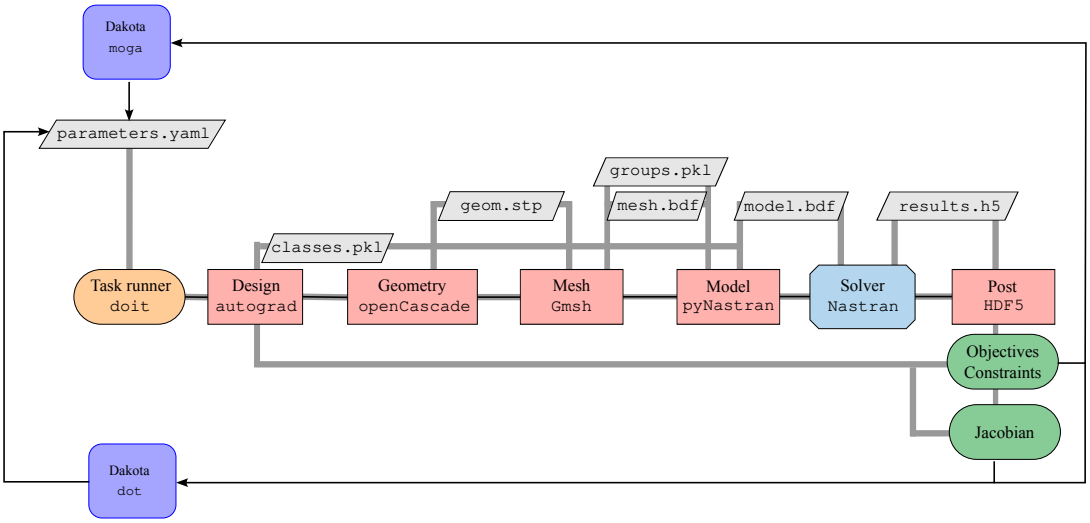

Fig 14. Implementation of the optimization process

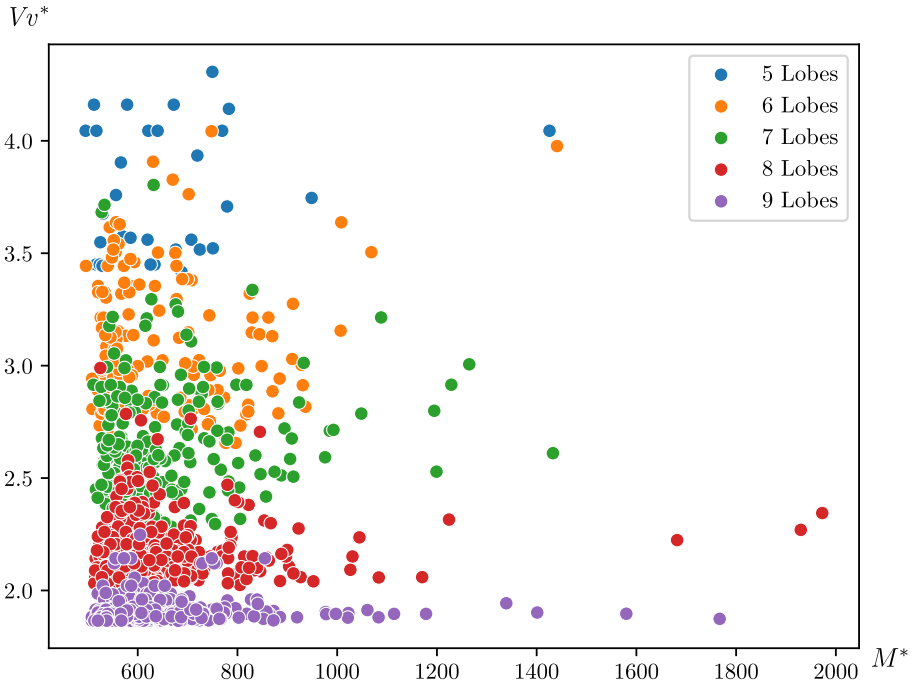

Fig 15. Results from global search optimization

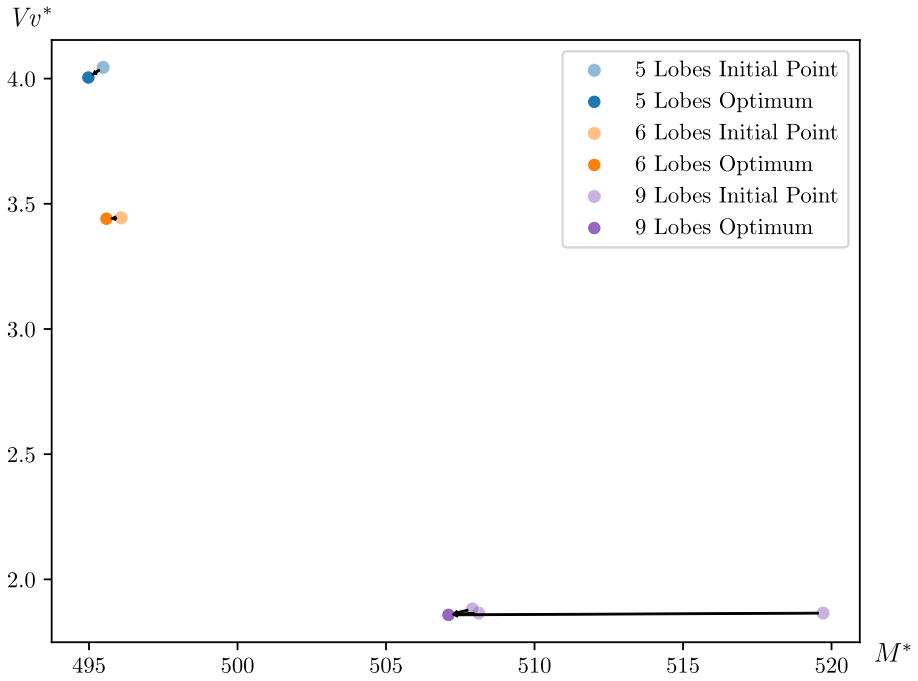

Fig 16. Results from local search optimization

Table 1. Number of lobes, void volume (Vv^*) and mass (M^*) in the optimum designs

Number of lobes	Vv^* (m^3)	M^* (kg)
5	4.004	491.98
6	3.440	495.58
9	1.858	507.10

optima ($Vv < 2$ in Fig. 16). The configurations in the cluster with lower mass ($M < 500$ kg in Fig. 16) exhibit lobes closer together in the narrowest part of the wing, and further apart towards the right bound. This is because the membrane stresses are smaller the smaller the lobe radius. The minimum mass design is a nine-lobe configuration, with lower gap between lobes. In this scenario, the outer mold line of the tank is closer to the outer mold line of the wing, hence less volume is wasted. However, the main drawback is that a higher number of webs is required, significantly increasing the mass of the multi-lobe configuration.

The optimization results demonstrate that the proposed approach performs trade-offs between volumetric and structural performance in an effective way, taking into account the chosen objectives. In this sense, a multi-functional design can now be adapted to any external shape.

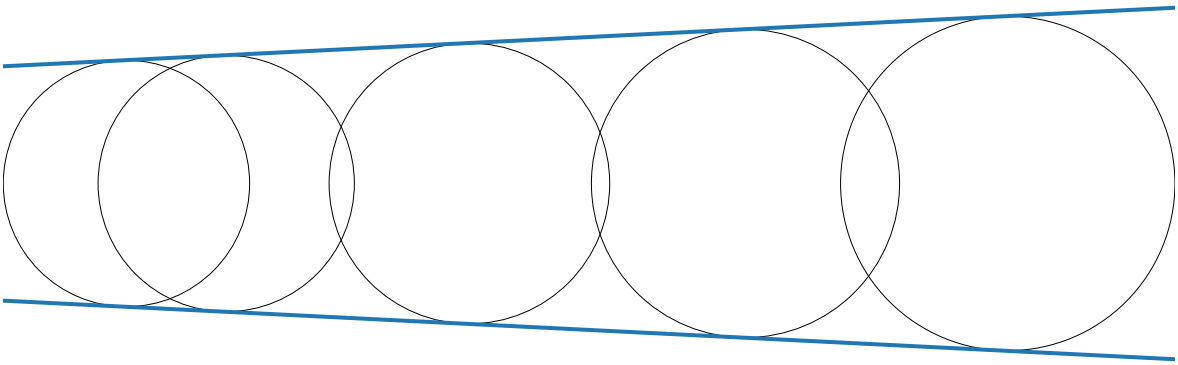

(a) 5 Lobes, $Vv^* = 4.004$ m^3, $M^* = 494.98$ kg

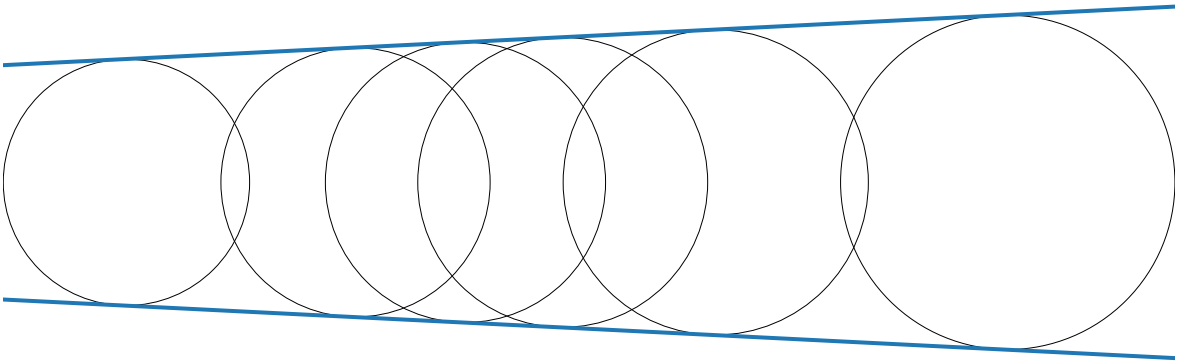

(b) 6 Lobes, $Vv^* = 3.440$ m^3, $M^* = 495.58$ kg

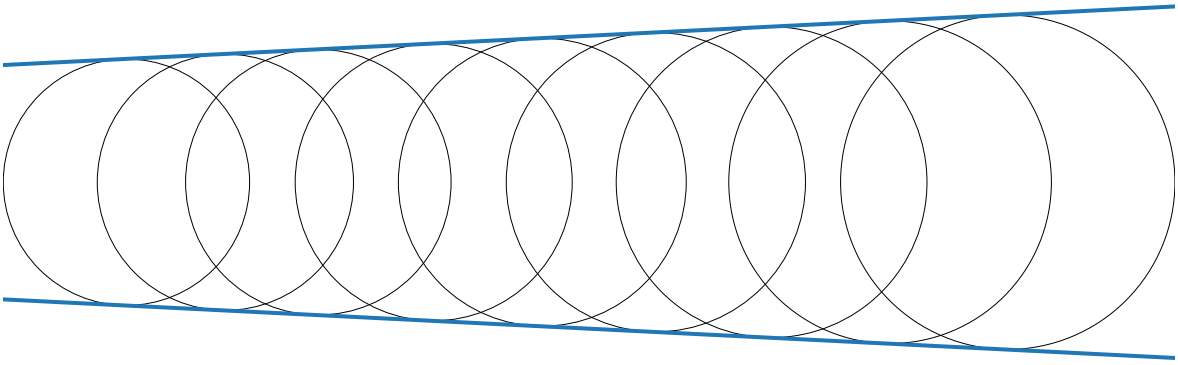

(c) 9 Lobes, $Vv^* = 1.858$ m^3, $M^* = 507.10$ kg

Fig 17. Lobe distribution for each optimum design

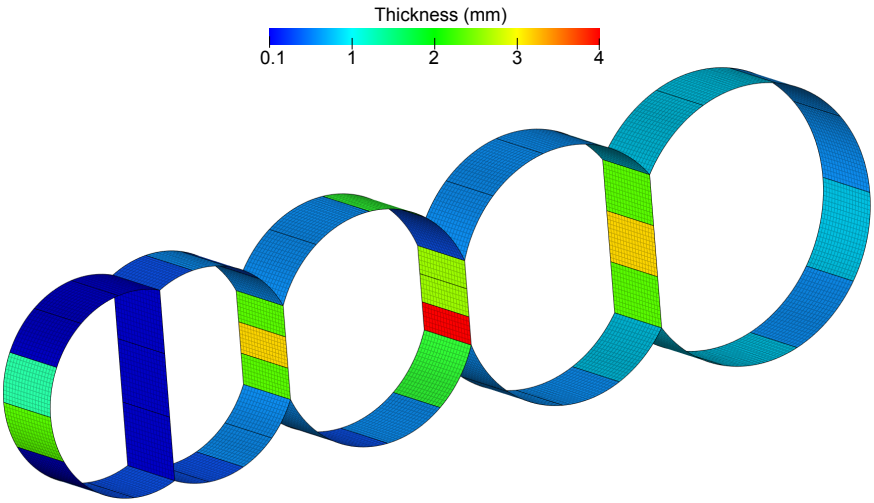

(a) 5 Lobes, $Vv^* = 4.004$ m^3, $M^* = 494.98$ kg

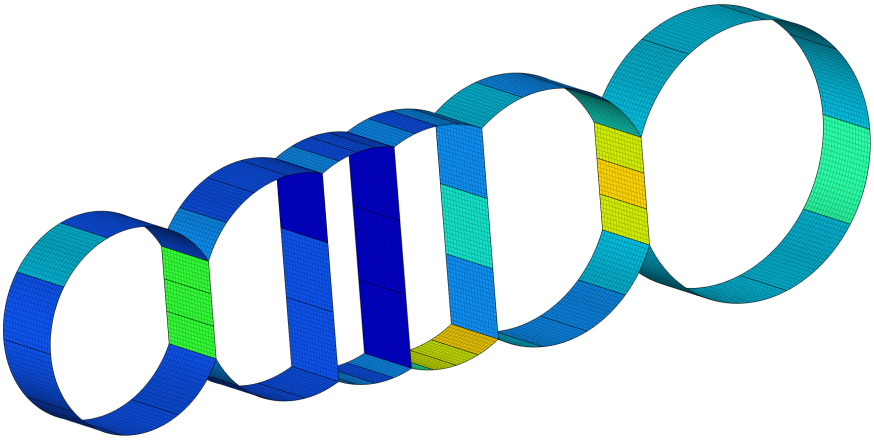

(b) 6 Lobes, $Vv^* = 3.440$ m^3, $M^* = 495.58$ kg

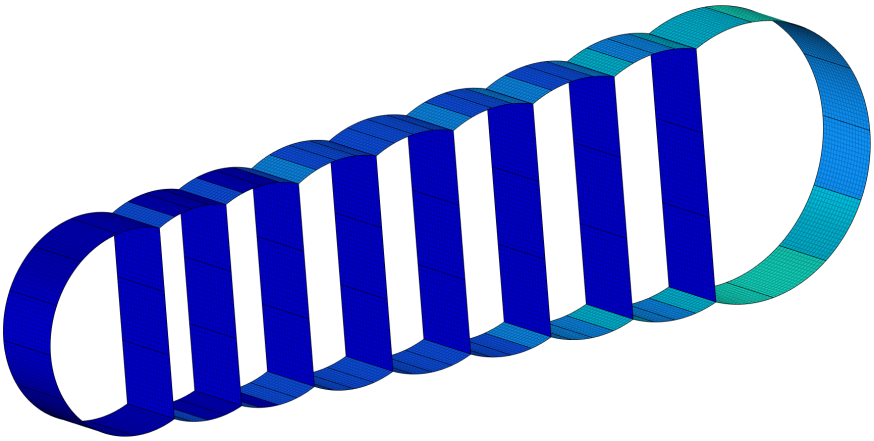

(c) 9 Lobes, $Vv^* = 1.858$ m^3, $M^* = 507.10$ kg

Fig 18. Thickness distribution for each optimum design

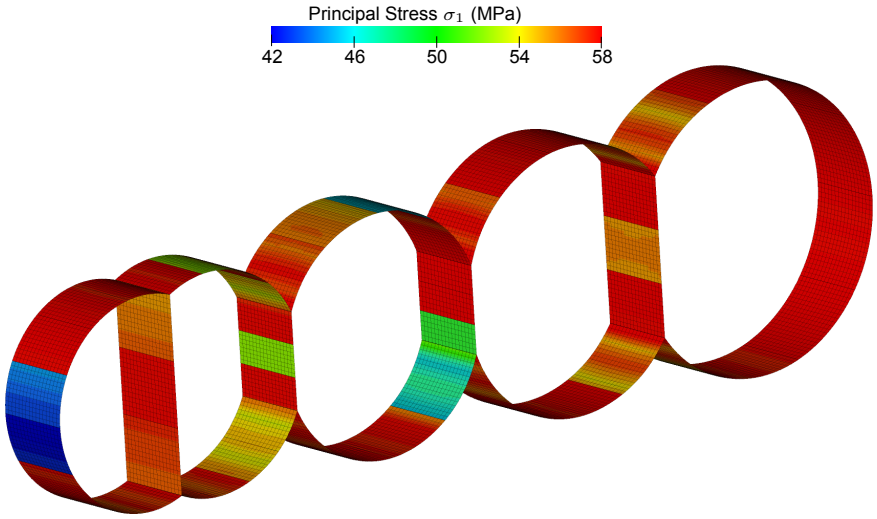

(a) 5 Lobes, $Vv^* = 4.004$ m^3, $M^* = 491.98$ kg

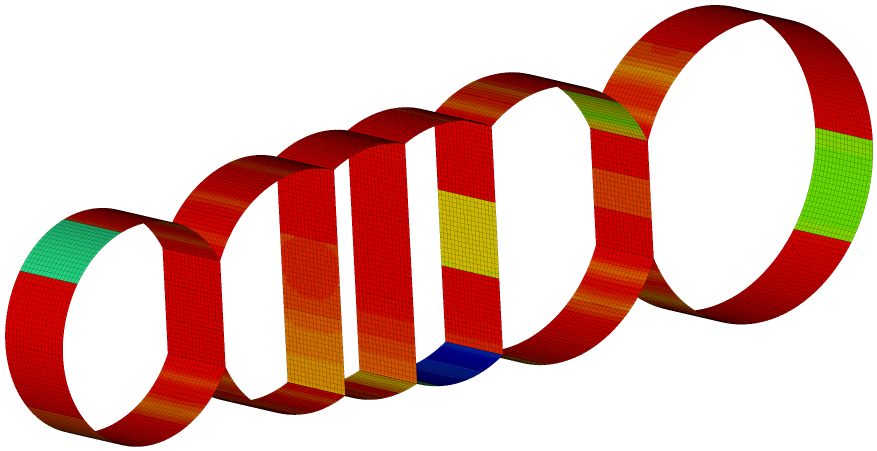

(b) 6 Lobes, $Vv^* = 3.440$ m^3, $M^* = 495.58$ kg

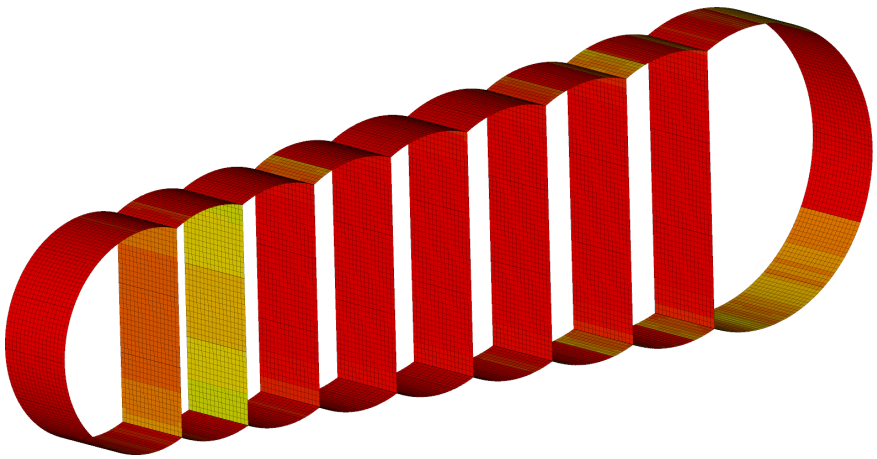

(c) 9 Lobes, $Vv^* = 1.858$ m^3, $M^* = 507.10$ kg

Fig 19. Stress distribution for each optimum design

7. Conclusions and future work

In this work, an approach to obtain optimum multi-lobe pressure tank configurations for hypersonic aircraft is presented. To this end, a multi-objective approach was performed to simultaneously minimize the tank weight and maximize its volumetric capacity. In a first stage, a parametric finite element model was developed to fit a wedge geometry representative of wave-rider wings. Then, the parametric model was incorporated into an optimization problem organized in two optimization levels: the outer level corresponds to the global search where several designs are proposed to explore the entire design domain. All of them are optimized using a gradient-based algorithm. As a result, a set of non-dominated designs are passed to the next optimization step, where the designs are improved.

The optimization was performed including pressure and aerodynamic loads relative to a cruise speed of $Ma = 8$ and $0°$ angle of attack. During the process, finite element meshes were generated automatically, where each mesh contains approximately $70\,000$ quadrilateral elements with bending and membrane properties. The optimization problem was solved using as design variables ten relative overlap positions and a non-fixed number of thickness variables that depend on the number of lobes. The von Mises stress of the aluminium was imposed as a constraint on all the elements of the skin and webs. The solution of these problems required 10 hours of wall time using 50 processors in parallel to solve the set of models. The computational cost was reduced by efficient derivative calculation integrated into gradient based algorithms combined with global search methods.

A Pareto front was obtained, providing insights into the structural and volumetric trade offs of a multi-lobe design. This is a promising approach for designing the tanks of not only hypersonic wave-riders, but other non-standard airplane configurations or heavy-lift launch vehicles. The interest in this topic is likely to continue as long as interest in hydrogen powered vehicles continues to rise, due to the high energy density of the hydrogen and its zero-emission combustion.

Future research will be focused on applying the methodology to the full LAPCAT wing, including tapering in the longitudinal direction of the tank. Additionally the parametric finite element model can be enhanced by including additional stiffeners, non-linear behaviour, and thermal loads and the dynamic effect of fuel sloshing.

References

[1] M. Ardema, “Structural weight analysis of hypersonic aircraft,” *Nasa Technical Report Server*, 1972.

[2] J. Steelant, R. Varvill, C. Walton, S. Defoort, K. Hannemann, and M. Marini, “Achievements Obtained for Sustained Hypersonic Flight within the LAPCAT-II project,” in *20th AIAA International Space Planes and Hypersonic Systems and Technologies Conference*, (Glasgow, Scotland), American Institute of Aeronautics and Astronautics, July 2015.

[3] M. Rodríguez-Segade, S. Hernández, and J. Díaz, “Multi-bubble scheme and structural analysis of a hypersonic stratospheric flight vehicle,” *Aerospace Science and Technology*, vol. 124, 2022.

[4] J. Steelant and M. van Duijn, “Structural Analysis of the LAPCAT-MR2 Waverider Based Vehicle,” in *17th AIAA International Space Planes and Hypersonic Systems and Technologies Conference*, (San Francisco, California), American Institute of Aeronautics and Astronautics, 2011.

[5] J. Malfroy, *Design and optimization of a tapered multi-bubble tank for hypersonic aircraft*. PhD thesis, KU Leuven, 2022.

[6] S. M. Aceves, F. Espinosa-Loza, E. Ledesma-Orozco, T. O. Ross, A. H. Weisberg, T. C. Brunner, and O. Kircher, “High-density automotive hydrogen storage with cryogenic capable pressure vessels,” *International Journal of Hydrogen Energy*, vol. 35, pp. 1219–1226, Feb. 2010.

[7] G. Letchworth, “X-33 Reusable Launch Vehicle Demonstrator, Spaceport and Range,” in *AIAA SPACE 2011 Conference & Exposition*, (Long Beach, California), American Institute of Aeronautics and Astronautics, Sept. 2011.

[8] J. Steelant and M. van Duijn, “Structural Analysis of the LAPCAT-MR2 Waverider Based Vehicle,” in *17th AIAA International Space Planes and Hypersonic Systems and Technologies Conference*, (San Francisco, California), American Institute of Aeronautics and Astronautics, Apr. 2011.

[9] J. N. Reddy, *An Introduction to the Finite Element Method*. McGraw-Hill Series in Mechanical Engineering, New York, NY: McGraw-Hill Higher Education, 3rd ed ed., 2006.

[10] W. L. Engstrom, “Determination of design allowable properties. Fracture of 2219-T87 aluminum alloy,” Tech. Rep. D180-14480-1, Mar. 1972.

[11] R. Ibrahim, *Liquid Sloshing Dynamics*, vol. 9780521838856 of *Liquid Sloshing Dynamics*. 2005.

[12] W. J. Gordon and L. C. Thiel, “Transfinite mappings and their application to grid generation,” *Applied Mathematics and Computation*, vol. 10–11, pp. 171–233, Jan. 1982.

[13] J. Martins and J. Hwang, “Review and unification of methods for computing derivatives of multidisciplinary computational models,” *AIAA Journal*, vol. 51, no. 11, pp. 2582–2599, 2013.

[14] U. Naumann, *The Art of Differentiating Computer Programs: An Introduction to Algorithmic Differentiation*. Software, Environments, and Tools, Philadelphia: Society for Industrial and Applied Mathematics, 2011.